Experimental assessment of thermal non-equilibrium (NEQ) in H_2-air detonations with emission spectroscopy

Hussein Bilal, Karl P. Chatelain, Deanna A. Lacoste

Mechanical Engineering Program, Physical Science and Engineering Division, King Abdullah University of Science and Technology (KAUST), Thuwal, 23955-6900, Saudi Arabia

Clean Energy Research Platform (CERP), King Abdullah University of Science and Technology of Science and Technology (KAUST), Thuwal, 23955-6900, Saudi Arabia

1 Introduction

The importance of thermal non-equilibrium (NEQ) in detonation has been discussed in previous studies due to their suspected role on chemical reactivity and cellular structures, from which experimental-numerical discrepancies could be attributed [1–4]. In the literature, different approaches have been employed to model this delayed reactivity by using simple two-temperature (i.e., Park model) or more complex state-to-state models in either one-dimensional (1D) steady or two-dimensional (2D) unsteady detonation simulations. Shi et al. [3] showed with different modeling approaches that the typical experimental-numerical discrepancies can be reduced, when NEQ effects are taken into account. Recently, Vargas et al. [5] conducted state-to-state 1D steady detonation modeling and reported two NEQ regions: one, mainly endothermic, in the induction zone caused by slow vibrational-translational relaxation, and an exothermic one at the reaction front, driven by chemical reactions. Despite all these numerical efforts, no clear experimental evidences of thermal NEQ were reported in previous studies, outside the indirect negligible evidences of Shi et al. [4] and Rojas Chavez et al. [6] from soot foil analyses and NO-LIF profile evolution, respectively. Outside of detonation studies, vibrational NEQ of hydroxyl radical (OH) has been reported both experimentally and numerically during the ignition behind a shock wave. Experimentally, vibrational temperatures two times higher than translational temperature [7] were reported in the reaction zone, while temperatures as high as 5000 K were reported numerically [8]. Among all the diagnostics available, emission spectroscopy is a powerful, non-intrusive, and relatively simple diagnostic to evidence thermal NEQ in many fields (e.g., plasmas, supersonic combustion, and hypersonic flows). However, no previous usage of emission spectroscopy on detonations was found in the literature.

This study aims to measure the emission spectra of H_2-air detonation for different initial pressures (25-100 kPa) and position behind the shock. First, species contributing to the emission spectra are identified. Then, experimental spectra are analyzed by comparison with simulated ones to evidence thermal NEQ of the emitting species.

2 Material and methods

Experimental setup The experiments were carried out with an optical detonation duct (ODD) measuring 3.75 m in length with a cross-section of $170 \times 40\,\text{mm}^2$. More details on the experimental configuration and procedures can be found in previous studies [9–11]. Table 1 summarizes the experimental conditions investigated in this study, as well as the characteristic length scales associated with each mixture, obtained from Zel'dovich-von Neumann-Döring (ZND) simulations. Details on ZND simulations are available in the next section (see Modeling tools).

Correspondence to: karl.chatelain@kaust.edu.sa

Table 1: Summary of the investigated mixtures and conditions. Characteristic length scales from ZND simulations: CJ detonation speed (D_{CJ}), vN and CJ temperatures (T_{vN} and T_{CJ}) and pressures (P_{vN} and P_{CJ}), induction zone length (Δ_i), averaged mole fraction in the burnt gases (x_{OH}), activation energy (θ), Ng stability parameter (χ), the Ng (λ_{Ng}) and experimental (λ_{Exp}) cell width. Simulations are conducted with SDT [12] considering 293 K initial temperature. *: data from [11].

Mixtures	**Pressure [kPa]**	**D_{CJ} [m/s]**	T_{vN}/T_{CJ} **[K]**	P_{vN}/P_{CJ} **[MPa]**	Δ_i **[μm]**	x_{OH} [-]	θ **[μm]**	χ **[-]**	λ_{Ng} **[mm]**	λ_{Exp} **[mm]**
2H2-O2-3.76N_2	25	1940	1492—2842	0.68—0.39	548	2.7%	4.8	2.0	26.1	13*
2H_2-O_2-3.76N_2	50	1956	1511—2895	1.39—0.78	268	2.3%	5.3	2.7	12.8	-
2H_2-O_2-3.76N_2	100	1971	1529—2946	2.82—1.59	143	2.0%	6.6	4.1	6.5	-

For each mixture, the chemiluminescence emitted by the detonation was collected by a 75-mm UV enhanced parabolic mirror (Thorlab CM750-075-F01, $f = 75$ mm) and focused at the entrance of a UV compatible optical fiber bundle (Princeton Instruments LG-455-020-3, 190-1100 nm). The optical fiber was connected to a spectrometer (Princeton Instruments Acton SP2300) to disperse light on the selected gratings. Two gratings, 150 and 600 grooves/mm, were employed to cover a wide and narrow wavelength range, respectively. Both presented a 300-nm Blaze wavelength. The dispersed light was then sent to an intensified CCD camera (Princeton Instruments PI-MAX4, Gen-II Sb intensifier, 1024x1024 pixels^2). A custom region of interest with vertical binning was employed to improve the signal-to-noise ratio, while maintaining a good spectral resolution. The spectral resolutions were 1.84 and 0.56 nm for the 150 and 600 grooves/mm gratings, respectively. Single-shot spectra were collected with a 10-µs exposure time and different gains to maximize counts without saturating the camera. All spectrum were obtained with the detonation in the middle of the field of view, except specified differently, and with the parabolic mirror collecting all the light from the visualization window.

Prior the measurements, the spectrometer was calibrated both in wavelength (Princeton Instruments IntelliCal, mercury lamp) and intensity (Hamamatsu L6565, deuterium lamp). For each condition, the emission spectrum was collected five times and post-processed: each spectrum was background corrected, the five spectra averaged, and the intensity normalized. Figure 1 illustrates the minimal variability between single-shot and averaged spectra, confirming that the averaging only minimizes the noise without hindering shot-to-shot variabilities.

Modeling tools The ZND simulations are performed with the Shock and Detonation Toolbox (SDT) [12] to obtain the characteristic length scales and post-shock detonation conditions for each pressure (see Table 1). Simulations are conducted with the chemical model of Mével et al. [13], which was previously validated and employed in detonation studies [14]. Emission spectra of OH A-X are simulated with the commercial code SPECAIR [15], using the experimental slit function. For each condition, the vibrational (T_v) and rotational (T_r) temperatures of OH are determined by fitting the experimental spectra, while the electronic (T_e) and translational (T_{tr}) temperatures are set at the CJ condition. For this reason, T_e and T_{tr} are not recalled in the result section, as both have no influence on the emission spectra when self-absorption is neglected. Similarly, the negligible effect of water (i.e., air moisture), O_2, and CO_2 in the ambient air has been confirmed for optical paths up to 10 times our actual one. However, a significant impact of the OH self-absorption was found for the present detonation conditions, such that different temperature fits could be obtained for the same CJ condition with and without this self-absorption feature (as presented in Fig. 2). In addition, similar fit performance could be obtained for very different thermal NEQ conditions if this option is omitted. With the self-absorption addition, T_e, T_{tr}, and the pressure can slightly impact the simulated spectra, while they were initially negligible. For each simulation, the self-absorption was included considering the burnt gas OH mole fraction (x_{OH}), computed from ZND simulation and reported in Table 1, and a 2-cm slab. This slab corresponds to the optical path and was set to match the half-width of the ODD.

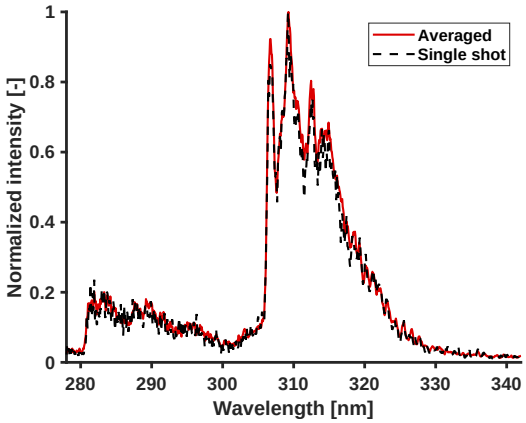

Figure 1: Comparison of averaged and single-shot spectra for H_2-air at 293 K and 50 kPa initial conditions.

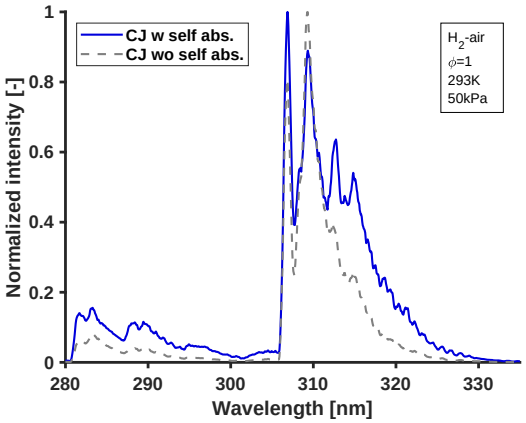

Figure 2: Differences in emission spectra when considering or neglecting OH self-absorption.

3 Results and discussions

3.1 Experimental spectra discussions

Figure 3 presents the reconstructed emission spectrum of a stoichiometric H_2-air detonation, under initial conditions 50 kPa and 293 K. This reconstructed spectrum, collected between 200 and 800 nm, is the result of multiple shots at different center wavelength (CWL) with a 150 grooves/mm grating. From Fig. 3, OH is the main species contributing to the spectrum, with the following vibrational bands: i) the most intense region near 310-320 nm corresponds to (0,0) and (1,1); ii) the second most intense region, near 280-295 nm, corresponds to (1,0), (2,1), and (3,2); iii) the two peaks at 345 nm correspond to (5,5) and (0,1); iv) the two peaks near 265 nm correspond to (2,0) and (3,1). Outside of these main vibrational bands of OH, the following two comments can be made: the signal obtained between 610-620 nm is a second-order diffraction of the (0,0) and (0,1) vibrational bands (i.e., 305-310 nm), which can be neglected. The broadband background contribution (i.e., 220-450 nm) appears to be mainly attributed to a convolution of the OH vibrational bands and marginally from interfering species (e.g., H_2O). Spectra with identical features were obtained at different pressures and gratings.

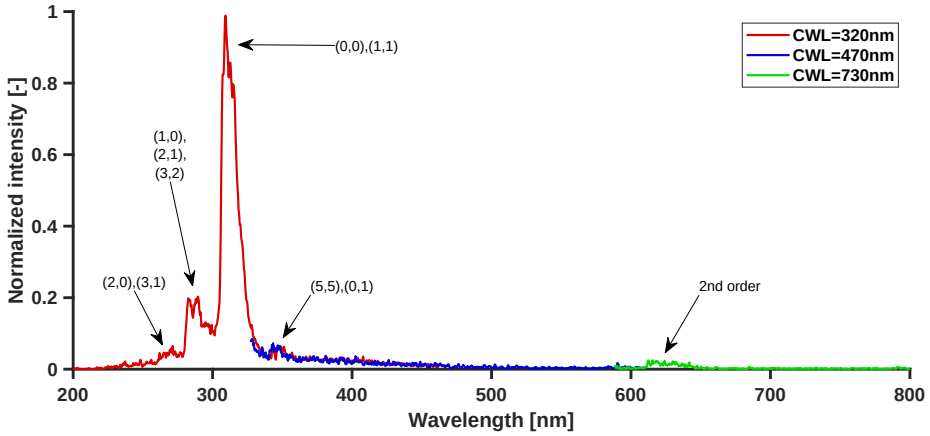

Figure 3: Typical emission spectra collected for a stoichiometric H_2-air detonation at 50 kPa and 293 K. This spectrum was obtained from multiple single-shot experiments at 320, 470, and 730 nm center wavelength (CWL) with a 150 grooves/mm grating. These spectra are not averaged. Annotations correspond to peak identification.

From these results,the following analyses will focus only on the most intense part of the emission spectra, corresponding to (0,0) and (0,1) vibrational bands, near 310 nm with a 600 grooves/mm grating.

Figures 4a and 4b present the evolution of emission spectra for stoichiometric H_2-air detonation with respect to initial pressure and for two locations within the detonation front, respectively. Figure 4a compares the normalized spectra for 25, 50, and 100 kPa detonations. Note that the emission spectra are qualitatively similar for P $\leq$ 50 kPa, while the spectrum differs significantly at 100 kPa. Figure 4b compares two emission spectra of stoichiometric H_2-air detonation, which are obtained at 50 kPa initial pressure and for two positions in the detonation front. The reference case, called "Front", refers to the emission spectrum at the detonation front (i.e., when the detonation is in the middle of the visualization window), while the "Burnt gas" case corresponds to 60 μs after the front has passed (i.e., corresponding to $\approx$ 12 cm behind the leading shock). All these relative positions and timing are confirmed with pressure signal traces (i.e., located before and after the visualization window), detonation speeds, and the camera opening signal. Variations in the emission spectra, observed in Figs. 4a-b, indicate small differences in the thermodynamic conditions of OH for different initial pressures and locations behind the shock. Both findings will be discussed in more detail in the next section by comparison with the simulated spectra.

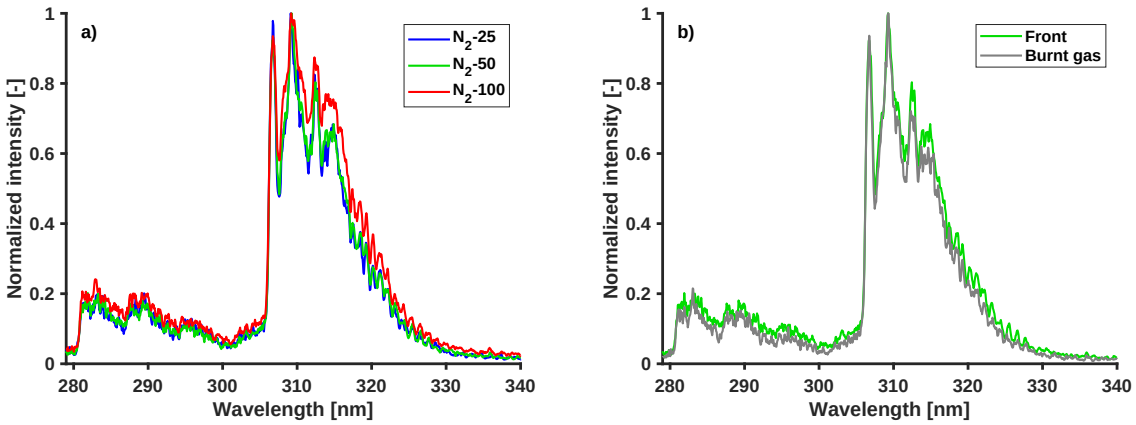

Figure 4: Evolution of the emission spectra of H_2-air detonations with initial pressure, in a), and with the position behind shock in b). Initial conditions in a) are $\phi = 1$, $T = 293$ K, and 25, 50, 100 kPa initial pressures. Initial conditions in b) are $\phi = 1$, $T = 293$ K, and $P = 50$ kPa.

3.2 Comparison with simulated spectra

This section aims to determine the thermodynamic conditions of the OH radicals by comparing the experimental spectra with four simulated spectra: i) a reference spectrum at CJ condition, where $T_{\mathrm{Tr}} = T_{\mathrm{V}} = T_{\mathrm{R}} = T_{\mathrm{CJ}}$; b) the best fit presenting thermal non-equilibrium (i.e., either vibrational, rotational, or both), where $T_{\mathrm{Tr}} = T_{\mathrm{CJ}}$ and $T_{\mathrm{V}} \neq T_{\mathrm{CJ}}$ and $T_{\mathrm{R}} \neq T_{\mathrm{CJ}}$; the best fit presenting thermal non-equilibrium, same fitting parameter as ii), with increased OH self-absorption $(x_{\mathrm{OH}} \times 2)$ contribution in iii) and without any OH self-absorption $(\sigma_{\mathrm{OH}} = 0)$ contribution in iv).

Figures 5a-c summarize the agreement of the four simulated spectra with the experimental ones at 25, 50, and 100 kPa initial pressures, respectively. Figures 5d compares the simulated spectra with the experimental ones for the "Burnt gas" condition (i.e., $\approx$ 12 cm behind the leading shock, which is outside the visualization window in this case) at 50 kPa initial pressure. From these figures, the following conclusions can be drawn: First, none of the experimental spectra seems to correspond to the CJ condition (in red); second, better agreement is systematically observed when vibrational NEQ only is included (in blue). Note that larger discrepancies are observed when considering rotational NEQ only or both

vibrational and rotational NEQ; third, the OH self-absorption significantly impacts the simulated spectrum. For the same vibrational temperature, the experimental-numerical agreement can be improved (in green) and decreased (in gray) when the OH self-absorption contribution is strengthened or removed, respectively. This further illustrates the extreme sensitivity of the emission spectra to OH self-absorption (see previous discussions in the Modeling tools in Section 2). Due to the strong spatial and temporal variations of thermodynamic conditions (i.e., temperature, pressure, x_{OH}) in detonations, the observed experimental-numerical deviations appear acceptable, and the determined vibrational temperatures are expected to be correct.

From these results we can report that vibrational temperatures are 700 to 1300 K above the translational temperature (T_{Tr}) at the detonation front case and are very close to the CJ condition ($\Delta T \leq 300$ K) far from the shock (see Section 3.1 for a detailed explanation of the difference between both cases). Both findings are consistent with previous findings on shock wave ignition or previous detonation modeling [5, 7, 8]. These findings confirm the expected vibrational excitation of OH in the reaction zone, via chemical reactions, followed by a vibrational-translational relaxation further downstream. In addition, it must be noted that thermal NEQ seems to increase with initial pressure and that vibrational-translational relaxation seems relatively slow after the reaction zone.

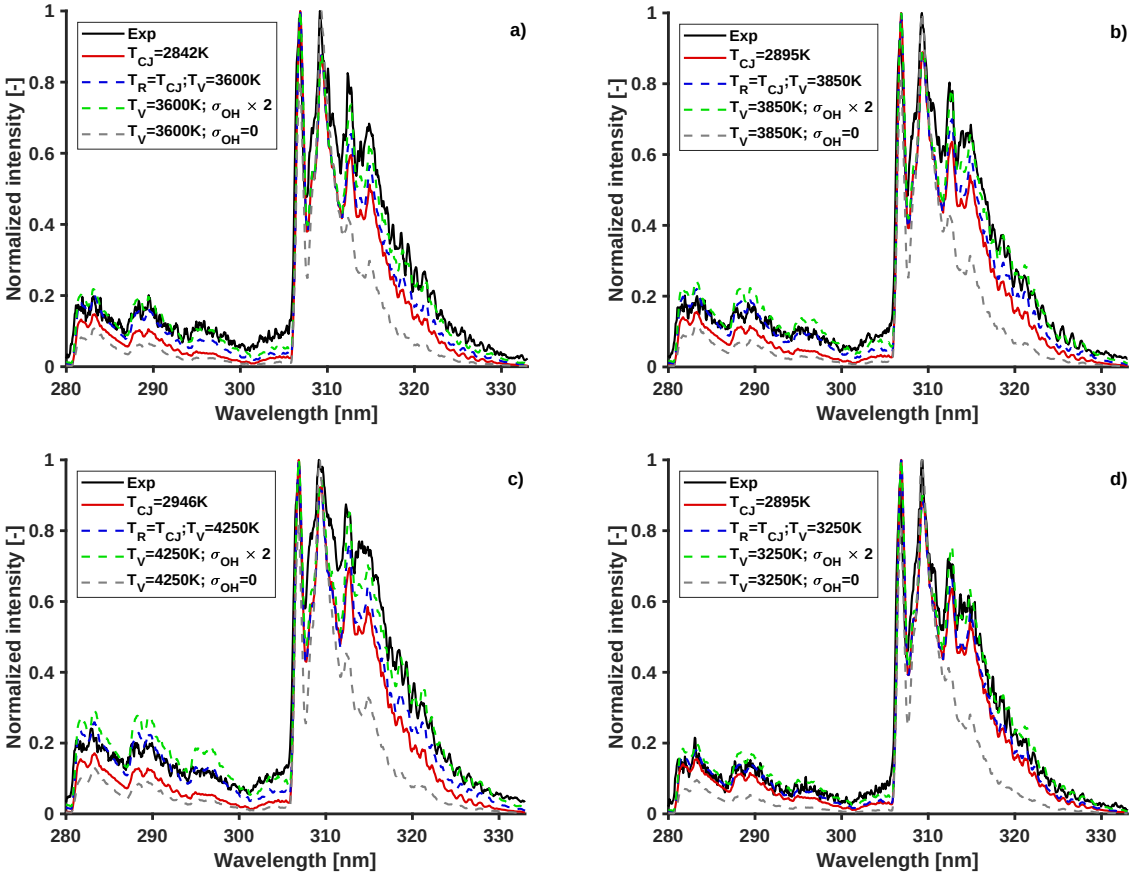

Figure 5: Experimental-numerical comparison of the OH spectra at different initial pressures (in a-c) and in the burnt gases (in d). The following emission spectra are computed: In red, the simulation considers equilibrium condition (CJ condition); In dashed blue, the simulation considers vibrational NEQ only (translational and rotational temperature at CJ condition); In dashed green, the simulation considers vibrational NEQ only (same as b) with increased self absorption contribution; In dashed gray, the simulation considers vibrational NEQ only (same as b) without self-absorption contribution.

4 Conclusions

This study measured the emission spectra of stoichiometric H_2-air detonations at initial pressures of 25-100 kPa and initial temperature of 293 K. Emission spectra were recorded from 200 to 800 nm and revealed the following: (1) only hydroxyl radical ($OH^\star$) chemiluminescence was observed for all conditions and no other significant species was identified. Thus, emission spectroscopy cannot be employed to characterize vibrational-translational relaxation of reactants (e.g. H_2, O_2, or N_2) in H_2-air detonations; (2) small differences in emission spectra were observed for different initial pressures and locations in the detonation front. After fitting of the spectra, the vibrational temperature of OH ($T_V(\mathrm{OH})$) was determined between 700 and 1300 K above the translational temperature at the detonation front, while vibrational temperatures very close to the CJ conditions (within 300 K) were observed downstream of the leading shock ($\approx$ 12 cm); (3) the experimental-numerical comparisons also evidence the critical importance of OH self-absorption in the emission spectra under our experimental conditions. These measurements provide the first experimental evidence of thermal NEQ in the reaction zone of a detonation, which needs to be consolidated with other techniques or experimental conditions due to possible uncertainties associated with the fitting procedures (i.e., OH self-absorption).

Acknowledgments

This work has been supported by the King Abdullah University of Science and Technology through the baseline fund BAS/1/1396-01-01. The authors thank J. Figueiredo, A. Alkhalifa, and M. Alicherif for their help with the first usage of the spectrometer.

References

[1] B. D. Taylor, D. A. Kessler, V. N. Gamezo, and E. S. Oran, "Numerical simulations of hydrogen detonations with detailed chemical kinetics," *Proc. Combust. Inst.*, vol. 34, no. 2, pp. 2009–2016, 2013.

[2] S. Voelkel, D. Masselot, P. L. Varghese, and V. Raman, "Analysis of hydrogen-air detonation waves with vibrational nonequilibrium," *AIP Conference Proceedings*, vol. 1786, no. 1, p. 070015, 2016.

[3] L. Shi, H. Shen, P. Zhang, D. Zhang, and C. Wen, "Assessment of vibrational non-equilibrium effect on detonation cell size," *Combust. Sci. Technol*, vol. 189, no. 5, pp. 841–853, 2017.

[4] X. Shi, A. S. Jayaraman, and H. Wang, "Probing vibrational nonequilibrium in detonations with ozone," *Proc. Combust. Inst.*, vol. 40, no. 1, p. 105695, 2024.

[5] J. Vargas, K. P. Chatelain, D. A. Lacoste, X. Huang, and R. Mével, *Non-Equilibrium Effects in H_2-O_2-Diluent Mixtures Using the ZND Reactor Model*. 29th ICDERS, SNU Siheung (Korea), 2023, Paper 78.

[6] S. B. Rojas Chavez, K. P. Chatelain, and D. A. Lacoste, "Two-dimensional visualization of induction zone in hydrogen detonations," *Combust. Flame*, vol. 255, p. 112905, 2023.

[7] F. E. Belles and M. R. Lauver, "Origin of oh chemiluminescence during the induction period of the h2–o2 reaction behind shock waves," *J. Chem. Phys.*, vol. 40, no. 2, pp. 415–422, 1964.

[8] O. V. Skrebkov, S. S. Kostenko, and A. L. Smirnov, "Vibrational nonequilibrium in the reaction of hydrogen with oxygen (review)," *Tech. Phys.*, vol. 69, no. 5, pp. 1378–1399, 2024.

[9] K. P. Chatelain, S. B. Rojas Chavez, J. Vargas, and D. A. Lacoste, "Towards laser-induced fluorescence of nitric oxide in detonation," *Shock Waves*, pp. 1–11, 2023.

[10] S. B. Rojas Chavez, K. P. Chatelain, M. Alicherif, and D. A. Lacoste, "Characterization of detonation waves by simultaneous OH and NO planar laser-induced fluorescence," *Appl. Energy Combust. Sci.*, vol. 18, p. 100257, 2024.

[11] M. Alicherif, S. B. Rojas Chavez, K. P. Chatelain, T. F. Guiberti, and D. A. Lacoste, "Experimental characterization of the cell cycle for multicellular detonations," *Combust. Flame*, vol. 266, p. 113553, 2024.

[12] S. Browne, J. Ziegler, N. Bitter, B. Schmidt, J. Lawson, and J. Shepherd, "Numerical tools for shock and detonation wave modeling," Explosion Dynamics Laboratory, GALCIT Pasadena, CA USA 91125, Tech. Rep., 2021.

[13] R. Mével, S. Javoy, F. Lafosse, N. Chaumeix, G. Dupré, and C.-E. Paillard, "Hydrogen–nitrous oxide delay times: Shock tube experimental study and kinetic modelling," *Proc. Combust. Inst.*, vol. 32, no. 1, pp. 359–366, 2009.

[14] V. Sankar, K. P. Chatelain, and D. A. Lacoste, "Evaluation of chemical kinetic models for simulations of hydrogen detonations by comparison with experimental data," *Appl. Energy Combust. Sci.*, vol. 21, p. 100306, 2025.

[15] SPECAIR, "Software package, ver. 3.0," *SpectralFit S.A.S.*, 2012.